2004 대한지구물리학회 · 한국물리탐사학회

공동학술대회 초록집

Proceedings of KGS · KSEG Conference

일시 : 2004년 6월 10일(목) ~ 11일(금)
장소 : 한국해양연구원 대강당

주최 : 대한지구물리학회, 한국물리탐사학회
후원 : 한국해양연구원, 한국학술진흥재단
한국지질조사탐사업협동조합

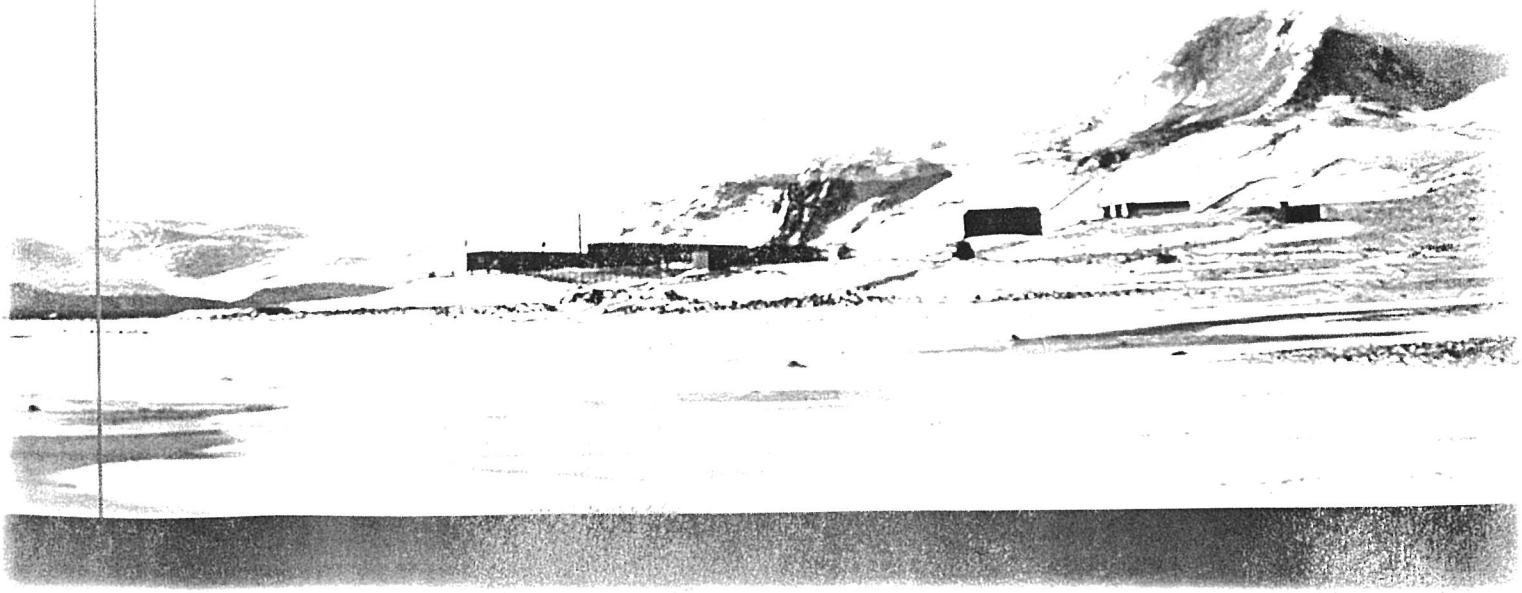

High-resolution seismic images of gas hydrate-bearing sediments in the Sea of Okhotsk

Y. K. Jin, S. H. Nam, K. H. Chung, J. Lee, Y. Kim

Korea Polar Research Institute, KORDI,ykjin@kordi.re.kr

1. Introduction

Gas hydrate-related features appear to be completely different images with respect to frequency [1,2]. For example, the bottom simulating reflectors (BSRs) occur as a sharp and strong reflector parallel to the seafloor on multichannel seismic profiles using low frequency seismic sources like airgun, whereas the BSR is not distinct or appears as diffuse high-amplitude reflections (HARs) around the base of the hydrate stability zone (BHSZ) on the profiles using high frequency sources like sparker or 3.5 kHz sub-bottom profiler. With the high-resolution seismic images obtained during the Leg 1 (cruise LV31) of the CHAOS project (2003) (Fig. 1), we examined gas hydrate- related features in gas hydrate-bearing sediments in the Sea of Okhotsk in this study.

2. The BSR

On all seismic profiles acquired using sparker (200-1200 kHz) during the CHAOS Leg1, the BSRs are generally not visible. The sharp and continuous reflector like the BSR occurs in the local area at the sub-bottom depth of 180 ms beneath the water depth of 1000-1050 ms in TWTT on the profile LV31-32-SA (Fig. 2).

3. The high-amplitude reflections (HAR) around the BHSZ

Instead, all profiles of Leg 1 reveal the HARs at the sub-bottom depth of 150-200 ms below the seafloor (Fig. 2). The HARs generally mimic the seafloor, and their depths coincide nearly with the BSR depths that are clearly defined on the nearby low frequency seismic profiles obtained by POI during KOMAX Project in 1999 [A. Obzhirov, personal communication]. Similar HARs were shown on several high-resolution seismic profiles of other study areas (i.e.

in Fig. 6 of Vanneste et al. (2001) and as ER in Figs. 4, 5 and 6 of Vanneste et al (2003)) [1,3]. The HARs are thought to be related to free gas present in pore space of the sediments beneath the hydrate stability zone [4].

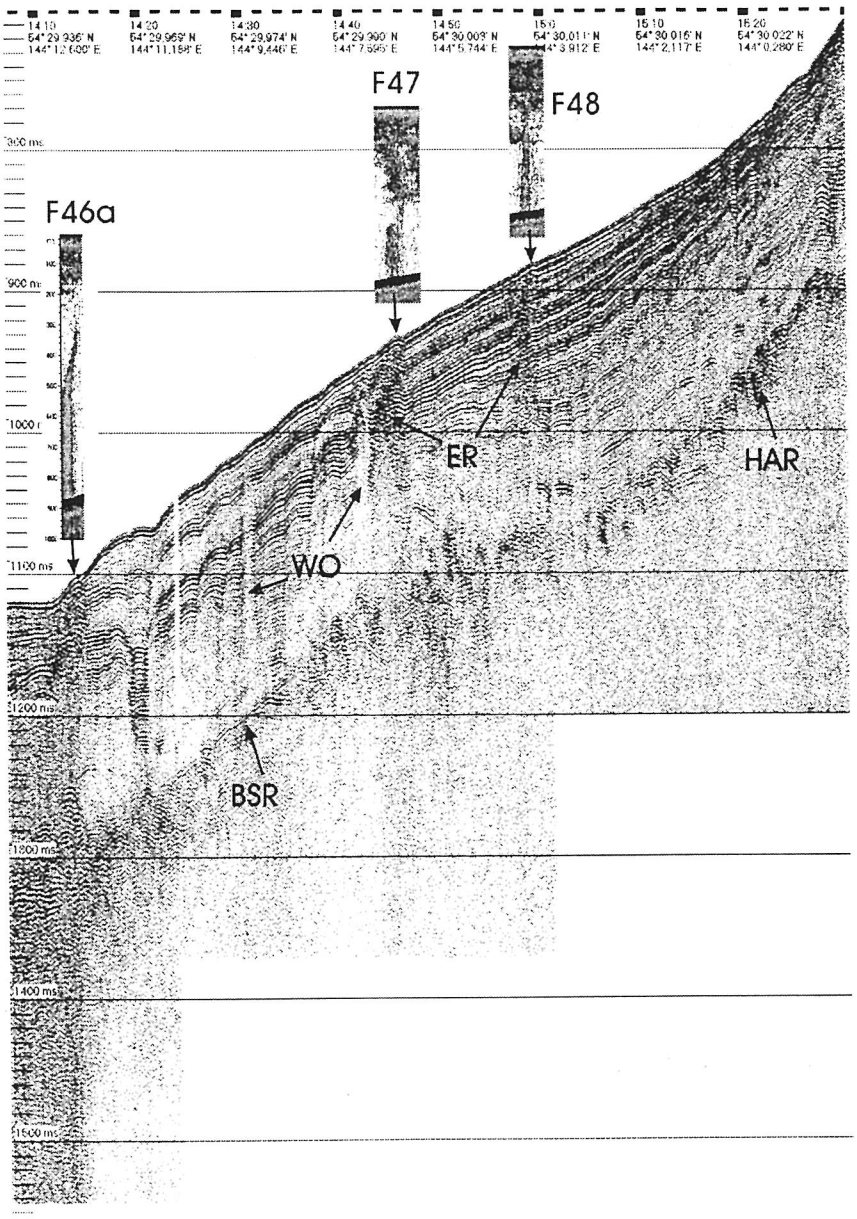

Fig. 2. High-resolution seismic profile of LV31-32. F46a, F47, and F48 (color insets) are gas flares. BSR: bottom simulating reflector, ER: enhanced reflection, HAR: high-amplitude reflectors, WO: wipe-out.

4. Wipeouts and enhanced reflection zones of the acoustic chimneys

All seismic profiles show many narrow near-vertical zones (acoustic chimneys) which seem to extend from HARs at the BHSZ near the seafloor or occasionally to intersect the seafloor. Most chimneys are associated with the bathymetric expressions. The chimneys show two different seismic reflection characteristics: (1) Some chimneys appear relatively narrower and white-colored vertical zone of little to no coherently reflected energy (wipeout: WO) as shown on profile LV31-21-2-SA. (2) Others show relatively wider and diffuse dark-color (enhanced reflection: ER) vertical zone as shown in profile LV31-32-SA (Fig. 2). Occasionally, some WO chimneys are converted to the ER chimneys near seafloor.

Wood et al. (2002) interpreted the WO chimney as gas chimney associated with upward heat and fluid flux, in which the seismic energy can be absorbed by gas [2]. But there are no velocity anomalies (like velocity pull-down) below the WO chimneys on the profile (Fig. 2), so the WO chimneys would be caused by amplitude blanking due to a saturation of gas hydrate.

The exact geological cause of the ER chimneys is ambiguous. The reflection pattern of the ERZ chimney is somewhat similar with that of the HAR at the BHSZ on the profiles. One possible interpretation is that the ER chimney could also be caused by free gas provided from a circuit (for example, faults) in the chimney along which heat and fluid flux migrates upward. Diffuse or alterative saturation of gas/gas hydrate would cause to enhance reflection of the sediments in/around the chimney.

We suggest that the occurrence of two different seismic reflections in the chimneys, the WO and the ERZ, could be controlled by certain parameters (concentration, physical properties etc) of gas/gas hydrates in the chimney.

5. Gas chimneys in sub-seafloor and gas flares in seawater

A lot of gas emanation sites from sub-seafloor into seawater, where gas bubbles form gas flares, have been discovered at the Sakhalin margin. The gas flares were also well detected during hydroacoustic survey (using mainly 12 and 19.7 kHz) of the CHAOS project.

With high-resolution acoustic and hydroacoustic profiles that were obtained on the same survey tracks, we examined the relationship between gas chimneys and gas flares. As shown on profile LV31-32-SA (Fig. 2), gas flares in the study area are very closely correlated with topographic expression above the ER chimneys. So it is noted that the ER chimneys are more strong active circuits of gas migration from sub-surface into the seafloor.

References

Venneste, M., De Batist, M., Golmshtok, A., Kremlev, and Versteeg, W., 2001, Muti-frequence seismic study of gas hydrate-bearing sediments in Lake Baikal, Siberia, Marine Geology, 172, 1-21.

Wood, W.T., Gettrust, J.F., Chapman, N.R., Spence, G.D, and Hyndman, R.D., 2002, Decresed stability of methane hydrates in marine sediments owing to phase-bounary roughness, Nature, 29, 656-660.

Venneste, M., Poort, J., De Batist, M., and Klerkx, J., 2003, Atypical heat-flow near gas hydrate irregularities and cold seeps in the Baikal Rift Zone, Marine and Petroleum Geology 19, 1257-1274.

Cooper, A. K., and Hart, P.E., 2003, High-resolution seismic-reflection investigation of the northern Gulf of Mexico gas-hydrate-stability zone, Marine and Petroleum Geology, 19, 1275-1293.

Altimetry-implied Free-air Gravity Anomaly of the Russian Arctic

Jeong Woo Kim*, Yeadong Kim, Sang Heon Nam**, Young Keun Jin**, Bang Yong Lee****

* *Dept. of Geoinformation, Sejong University.*
** *Polar Research Institute, Korean Ocean Research & Development Institute.*

Satellite radar altimeter observations have been increasingly used to determine free-air gravity anomalies (FAGA) of the remote regions of the Earth, such as the Arctic. In this paper, the ERS1 (The 1st European Remote Sensing Satellite) radar altimeter data were used to predict the FAGA of the Barents and Kara Seas in the Russian Arctic between the area 20° - 70° E and 68° - 78° N.

There are two different approaches for deriving FAGA from satellite radar altimetry. In the first approach, vertical deflections of the undulation data are used to calculate FAGA [Sandwell, 1990; 1992]. The benefit of this approach is ostensibly that it is not necessary to do orbital and cross-over adjustments, because the gradient solutions are being used. However, this approach distorts the regional anomalies that may be important in studying large-scale crustal features, and includes track-line noise in its predictions.

The other approach of Kim [1996] derives solutions directly from geoid undulations using the fundamental equation of geodesy and Brun's formula [Heiskanen and Moritz, 1967]. This method incorporates orbital cross-over adjustments and spectral correlation filtering of neighboring orbital data, as well as maps from ascending and d Fig. 1. ERS1 168-day mission data coverage of Barents and Kara Seas: Panel A represents ascending and Panel B represents descending tracks escending data sets to obtain the best possible estimate of the geoid undulation. This approach enhances the recovery of gravity at all wavelengths, because it is based on determining geoid undulations as accurately as possible. Furthermore, this approach permits procedures to be implemented in the wavenumber domain that are effective for attenuating track-line noise [Kim et al., 1998], especially at high latitudes where ascending and descending orbits cross each other at high angles.

Therefore, this study considered the second method and related improvements for enhancing the recovery of FA gravity anomalies of the Barents and Kara Seas between 20° - 70° E and 68° - 78° N from the 168-day mission of the ERS1. Kim and Roman [2001] already estimated FAGA of the Barents Sea using ERS1 168-day mission data with a reference FAGA grid from the Andersen and Knudsen [1998]'s global model [AKGM]. This study, however, was focused on the more detailed data processing techniques for calculating gravity anomalies from dense altimeter data of the study area. The estimated FAGA will be compared with AKGM and shipborne gravity obtained by Lamont-Doherty Earth Observatory of Columbia University to verify the validity of result.

DATA PROCESSING

As mentioned above, the approach of Kim [1996] was initially implemented to derive FA gravity anomalies directly from geoid undulation (GU) estimations. This method was completely updated to enhance the overall quality of the predictions. This approach uses a remove-and-restore technique with a gravimetric reference field. Residuals were generated by the differencing undulations observed by satellite relative to the reference undulation model (e.g., OSU91A from Rapp et al. [1991]). These undulations were then manipulated to generate residual FA gravity anomalies. Finally the reference gravity anomalies were added back to the residual gravity anomalies to create total FA gravity anomaly predictions.

Pre-Processing

The first step was to analyze the quality of the data points and apply corrections to the one-second observations. Most of the correction terms were determined from various models provided with the data. These correction terms could also be used to assess the quality of the data. Extreme values in significant wave height, for example, could be indicative of an unreliable observation point.

Several correction terms, such as dry and wet tropospheric corrections were used to determine the retained data points for further analyses. The tracks were grouped into ascending and descending data sets, based on their local times. This partitioning is essential for performing 1-D WCA. Fig. 1 gives the original data sets. There were 115,309 ascending (Panel A) and 116,163 descending observation points (Panel B).

Reference GU values were derived from the OSU91A spherical harmonic gravity model, with coefficients to degree and order of 360 [Rapp et al., 1991], and removed from observed values. Static components of the sea surface topography were determined from OSU91 global spherical harmonic model [Kim and Rapp, 1990], with coefficients to degree & order of 10, and also removed.

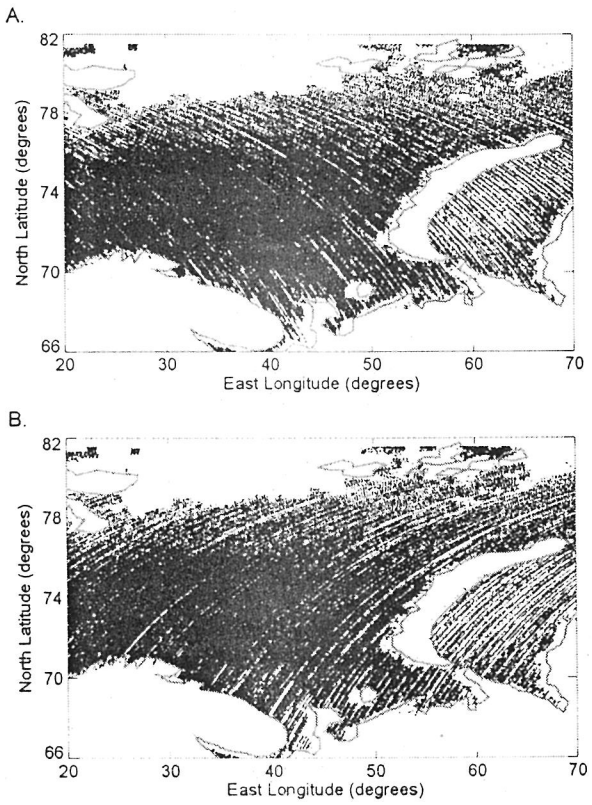

Fig. 1. ERS1 168-day mission coverage of Barents and Kara Seas: Panel A represents ascending and Panel B represents descending tracks.

Co-Linear Track Analysis

After having selected reasonable observation points, the tracks that were composed of these points were then analyzed for coherent signals that should include geologic information. The observation points were separated into groups of ascending and descending tracks. The interval of the data points in a track is one second, which is about 7 km along the ground track. Therefore, the tracks should be composed of observation points at 7 km intervals. However, some data points are missing due to altimeter errors, presence of landmasses, etc. Therefore, those tracks that had gaps of more than 60 % of overall length were pruned out. Additionally, tracks that are less than 20 km in length were of limited use for analysis and also eliminated.

As was mentioned earlier, track pairs must be geographically adjacent and sub-parallel to perform 1-D WCA. Therefore, tracks were geographically ordered within each set of ascending and descending tracks using a sorting latitude, such as 75°N for the Barents and Kara Seas area. Similar to the Magsat data processing, these two data sets were processed separately until they are combined in the final stage of the analysis. Also, the common components were extracted from the track pairs using WCA and assigned to locations in the middle of the original track pairs.

The above steps, however, do not reduce long-wavelength orbit errors. The orbit of the satellite varies slowly over time. If the research area is less than a 1,000 km in either direction, the satellite orbit errors may be assumed to be constant for each orbit for that area [Kim, J.H., 1996]. Hence, a least-squares orbit adjustment (i.e., cross-over adjustment) may be performed at cross-over points between ascending and descending tracks [Knudsen, 1987]. The two sets of orbital track data were combined so that most of the satellite orbit errors and dynamic sea surface topography (SST) were removed. After the adjustment, the ascending and descending tracks again were separated for further processing. Here, the tracks, either too short in total length or with too many gaps, were pruned out. The tracks were pruned out if the total number of missing points was more than 20% of the number of observation points in a track, or if the total number of the data points were less than 50. However, most of the pruned-out tracks were kept separately and used later for cross-over adjustment, because values of the data points in the pruned tracks are generally accurate enough to be used for reducing long-wavelength orbit errors.

Once the cross-over adjustment is completed, the retained data points were divided again into ascending and descending groups, and co-phased data points in each track are interpolated back to the original data spacing. The distance between back-interpolated data points in a track, therefore, should be very similar to the original observation data spacing in the track, and these points are used to predict GUs of the Barents and Kara Seas.

Map Analysis

The SSHs, termed residual GUs, were gridded using a tensioned cubic spline. The selected grid spacing was 15 minutes in longitude and 5 minutes in latitude in general conformance with the original data spacing. Additionally, the area was sub-divided into west and east sectors to make the analysis more manageable. As a result, the longitude ranges of the west and east data sets were between 20° to 55° E and 35° to 70° E, respectively. The 20° overlap was made to reduce edge effects when the data sets were recombined. Although the CCs (Correlation Cefficients) between ascending and descending data of the west and east regions were 0.859 and 0.946, respectively, the orbit errors were not completely removed in the cross-over

adjustments, as was evidenced by along-track lineation (i.e., washboard effect) in the residual GUs. The close track spacing of the 168-day mission data set results in an exaggeration of remaining orbit errors when the radial derivatives were taken. Simple averaging of the ascending and descending data sets in the data domain are only partly effective in eliminating these lineations. Differencing the wavenumber transforms of the ascending and descending data reveals contaminated quadrants where the data energy orthogonal to the track directions is represented.

In recovering the FA gravity anomalies from altimetry data, it is very important to determine accurate GUs from the ascending and descending altimetry observations. The combined GUs are obtained by merging ascending and descending GUs and the FA gravity anomalies will be directly calculated from the vertical derivative of the low-pass filtered (LPF) GUs (i.e., Eq. 2). In this study, the ascending and descending data sets are relatively well correlated (i.e., CCs are 0.859 and 946, respectively), but still need to be adjusted for non-lithospheric components. This additional effort may be able to eliminate residual errors that have not been removed. Instead of least-squares correction technique described in the Magsat data processing [Kim, 2002], a 2-D WCA was applied to the ascending and descending GU data sets. By doing this, the CC of the two data sets is enhanced and more stable GUs may be acquired.

From this point, the data analysis diverges from that approach taken by previous studies (i.e., Kim, [1996]). Without making any additional adjustment effort, previous method eliminated these lineations by extracting the two uncontaminated quadrants from each data set and recombining them into a complete transform, as discussed in Kim [2002] and Kim et al. [1998]. This study, however, correlated the ascending and descending data sets in the wavenumber domain (2-D WCA). Cut-off CCs of 0.86 and 0.96 were selected for the west and east data sets, respectively, based on the output power variations with increasing CC. By applying 2-D WCA, the CC between ascending and descending data of the western sector was increased by about 11%, while the CC of eastern sector was increased by slightly more than 4%. As a result, in both the western and the eastern maps, the lineations were greatly reduced with relatively minor losses of anomaly energy.

The adjusted (i.e., WCF'd) GUs were obtained then merged to produce combined GUs by quadrant-swapping method [Kim et al., 1998]. The residual GUs were finally combined and low-pass filtered for wavelengths two times greater than the grid interval (GI) to remove high frequency effects. The LPF GU maps do not appear to show any lineations and other high frequency effects related to the orbit tracks, as shown in Fig 2.

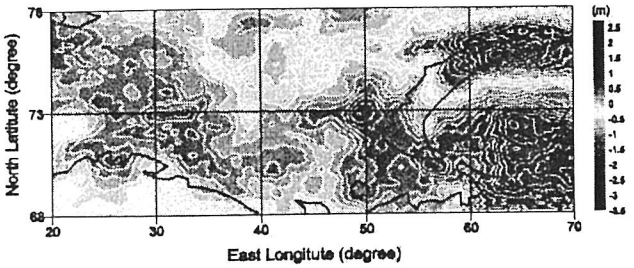

Fig. 2. Geoid undulations of the Barents and Kara Seas estimated from ERS-1 168-day mission radar altimeter data.

Predictions of Free-air Gravity Anomalies

The residual FA gravity anomalies can be calculated from the residual GUs shown in Fig. 2 using Brun's Formula and Fundamental Equations of Geodesy. Kim [1996] calculated the radial derivatives with FFT in spherical coordinates (φ,λ), assuming the spherical coordinate data had approximately the same station spacing in km in each direction. This assumption may result in unnecessary distortions particularly in the high latitude region [Kim and Lee, 2002]. In this study, therefore, the LPF averaged residual GUs were transformed to an (X,Y) plane using a Lambert Conformal Conic Projection. Then the vertical derivative was taken to generate residual FA gravity anomalies and projected back into spherical coordinate (φ,λ). The residual FA gravity anomaly maps are shown in Fig. 3. To produce the final total FA gravity anomalies, the reference FA gravity anomalies from the OSU91A gravity model, with coefficients to degree and order of 360 [Rapp et al., 1991](Fig. 4) were added back to the residual FA gravity anomalies (Fig. 5).

COMPARISON OF FREE-AIR GRAVITY ANOMALIES

To verify the validity of the estimated altimetry-implied FAGA, the final result in Fig. 5(C) was compared with the Andersen and Knudsen [1998]'s global model [AKGM] and shipborne gravity survey results by Lamont-Doherty Earth Observatory of Columbia University [NGDC, 1998]. The AKGM is the global model calculated from various satellite altimeter mission data such as Geosat GM as well as other lower altitude observations.

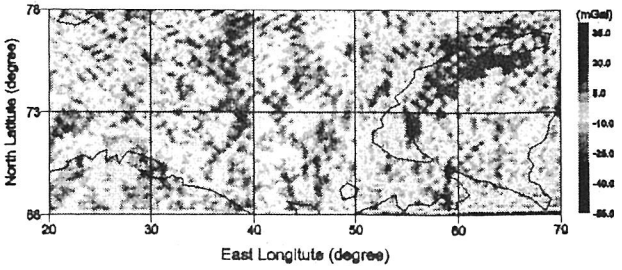

Fig. 3. Residual free-air gravity anomalies from geoid undulations in Fig. 2.

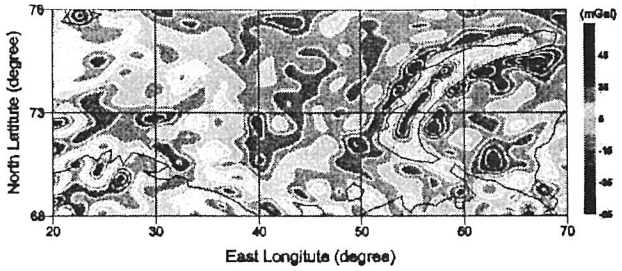

Fig. 4. Reference free-air gravity anomaly from the OSU91A gravity model, with coefficients to degree and order of 360 [Rapp et al., 1991].

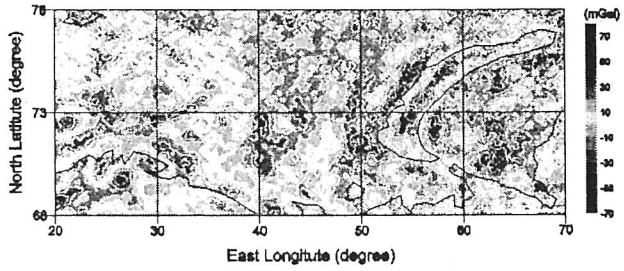

Fig. 5. Total (residual + rerference) free-air gravity anomaly derived from ERS1 168-day satellite radar altimeter data.

For graphical comparison, the two models and the differenced components are shown in Fig. 6. Overall, AKGM in Fig. 6 is smoother than the ERS1-168, and this is because AKGM was low-pass filtered to well present the long-wavelength components for global scale. In the differenced components in Fig. 7, major differences appeared near shores, such as in the northern coast of Novaya-Zymlaya Island, which deteriorated the CC between the two models. As shown in Table 1, the minimum and maximum values of the two models are quite different. This may be explained by the fact that altimetry-implied FAGA are effective for ocean area, while AKGM was estimated with land observations.

One of the possible explanations for big differences in the middle southern Kara Sea is lack of data. Many tracks were pruned out in this region because they were either too short in total length or with too many gaps, or some tracks were pruned out if the total number of the data points were less than 50.

The ERS-1 and AKGM anomalies in Fig. 6 were then compared with shipborne gravity values measured by Lamont-Doherty Earth Observatory of Columbia University [NGDC, 1998] in 1973 to verify the validity of result. The ERS-1 and AKGM gravity values were extracted along the Line #1 and #2 in Fig. 6 and Fig. 5 that were measured between Sep. 2 and 6, and Sep. 12 and 14 in 1973, respectively. The gravity anomaly profiles along the Lines #1 and #2 are shown in Fig. 7 (A) and (B). Statistically, the ERS-1 and AKGM profiles of Line #1 show CCs of 0.799 and 0.965 respectively with the shipborne profile, while those of Line #2 show lower CCs of 0.770 and 0.919, respectively. The CCs between ERS-1 and AKGM were 0.827 and 0.840. In particular, the shipborne gravity values were about 10-20 mGals higher than the other two models along the profiles. This may be because of the various reference ellipsoids used in the different gravity data processing.

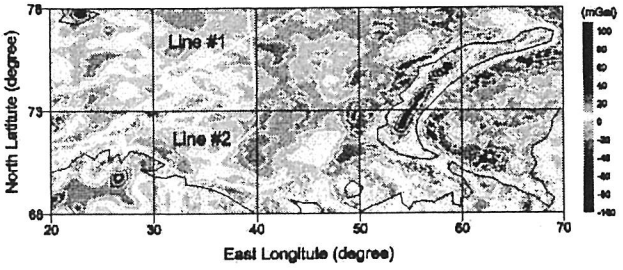

Fig. 6. Free-air gravity anomalies from Andersen and Knudsen[1998]'s global model. White dots denote shipborne survey lines #1 and #2 by Lamont-Doherty Earth Observatory of Columbia University, respectively.

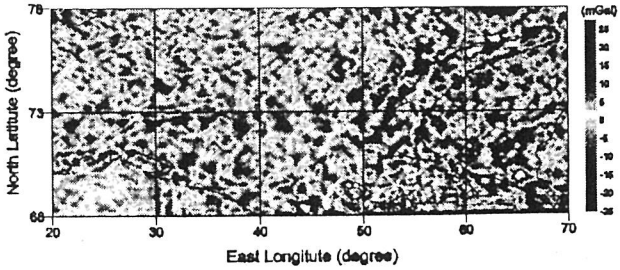

Fig. 7. Differenced (Fig. 6 – Fig. 5) free-air gravity anomaly of the study area.

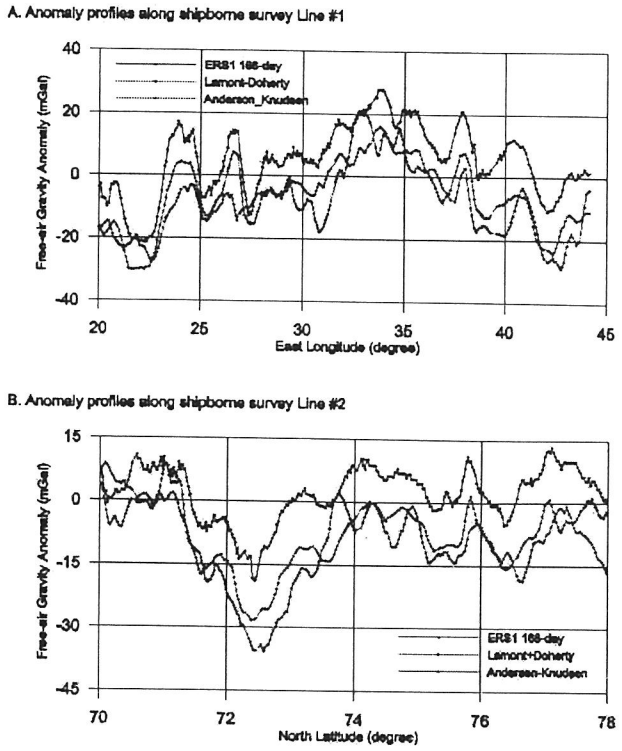

Fig. 8. Free-air anomaly profiles along shipborne survey lines #1(A) and #2(B) in Fig. 6. Red, blue, and green lines denote anomaly profiles for ERS1-168-day mission, shipborne measurements by Lamont-Doherty Earth Observatory, and Andersen and Knudsen [1998]'s model, respectively.

CONCLUSIONS AND DISCUSSIONS

We estimated free-air gravity anomaly (FAGA) of the Barents Sea and Kara Sea of the Russian Arctic between the area 20° - 70° E and 68° - 78° N from dense ERS1 168-day radar altimeter mission data. Geodetic co-phasing adjustment and 1-D Wavenumber Correlation Filtering (WCF) were applied to reduce possible distortions in the along-track data resampling for extracting common components using FFT. Local cross-over adjustments on the orbits were carried out by splitting the study into 2 groups, West (20° - 55° E) and East (35° - 70° E), to reduce distortions due to limitations of the planar cross-over adjustment.

Four sets of measurements were gridded from ascending and descending sets of West and East groups of tracks with tensioned splines, and 2-D WCFs between descending and ascending data sets were performed based on the ratio of retained-power vs CC spectrum, resulting in adjusted descending and ascending data sets. To estimate geoid undulation of the study area, the adjusted descending and ascending data were point-by-point averaged, resulting in base maps for the West and East groups. Low-pass filtering was then applied, which resulted in final geoid undulations for the two groups.

To estimate the residual FAGA from geoid undulations, Lambert Conformal Conic projection was adapted to project data on to X-Y plane before the radial derivative filter was applied for the two groups. The West and East FAGA were then combined to predict residual FAGA and, finally, the OSU91A gravity model (highest degree and order of 360) [Rapp et al., 1991] was added to the residual anomaly (Fig. 3), resulting in the total FAGA, which is the final result of this study (Fig. 5).

Barents and Kara Seas FA gravity anomalies presented in this study were compared statistically with the Andersen and Knudsen[1998]'s global model and shipborne measurements by Lamont-Doherty Earth Observatory of Columbia University. The correlation coefficient (CC) with the global model was 0.785 and CCs with two shipborne measurements were 0.799 and 0.770, respectively. In general, the altimetry-implied FAGA showed good coherence in the open sea, but along the coastline, there were mismatches with the global model.

FAGA map shown in Fig. 5 provides complete coverage for Barents and Kara Seas. It is derived from dense ERS1 168-day satellite altimeter mission data where the processing has been adapted to deal with problems resulting from the high latitude area, such as gaps by ice coverage, variability of angles between the direction of the ascending and descending tracks, and the distortions due to the Earth's spherical coordinates. Regional FAGA, such as derived from the radar altimetry, can be used to augment geologic analyses of correlative magnetic data by Poisson's Theorem [Kim, 1996]. Also, in conjunction with the accurate bathymetry, analyses of meteorite impact structure, isostatic rebound, and other tectonic features are possible.

ACKNOWLEDGMENT

This study was supported by research projects with a title of 'Arctic Atmospheric Environment and Mineral Resources Research' (PN47500) and other title of 'A Study on the Arctic Environmental Characteristics (PP03108)' of Korea Ocean Research and Development Institute (KORDI).

REFERENCES

Andersen, O.B., and P. Knudsen (1998) Global marine gravity field from the ERS-1 and Geosat

geodetic mission altimetry, J. Geophys. Res., 103, C4, p.8129-8138.
Heiskanen, W. A. and H. Moritz (1967) Physical Geodesy, W.H. Freeman and Company San Francisco, 364p.
Kim, J.W. (1996) Spectral Correlation of Satellite and Airborne Geopotential Field Measurements for Lithospheric Analysis, Ph.D. Dissertation (unpubl.), Department of Geological Sciences, The Ohio State University, Columbus, Ohio, 171p.
Kim, J.W. (2002) Recovery of Lithospheric Magnetic Components in the Satellite Magnetometer Observations of East Asia, Korean J. of Geophysical Exploration, 5(3), 157-168, 2002.
Kim, J.W. and D. Roman (2001) Improved Free-air Gravity Anomalies by Satellite Altimetry, Korean J. of Remote Sensing, 17(4), p.297-305.
Kim, J.W., J.H. Kim, R.R.B. von Frese, D.R. Roman, and K.C. Jezek (1998) Spectral attenuation of track-line noise, Geophys. Res. Lett., vol.25, No.2, 187-190.
Kim, J.W. and D.C. Lee (2002) Distortions of spherical data in the wavenumber domain, Korean J. of Remote Sensing, 18(3), 171-179.
Kim, J.-H. and R. Rapp (1990) Major datasets and fields in the area of gravimetric and altimetric research, OSU Internal Report, Department of Geodetic Sciences and Surveying, The Ohio State University, Columbus, Ohio.
Kim, J.-H. (1996) Improved Recovery of Gravity Anomalies from Dense Altimeter Data, Report No. 437, Department of Geodetic Science and Surveying, The Ohio State University.
Knudsen, P. (1987) Adjustment of satellite altimeter data from cross-over differences using covariance relations for the time varying components represented by Gaussian functions, Proc. IAG Symposia TOME II, p. 617-628.
NGDC (1998) Marine trackline geophysics data CD-ROM set, U.S. Dept. of Commerce, NOAA, National Geophysical Data Center, Boulder, Colorado.
Rapp, Richard, Yan Ming Wang, and Nikolaos K. Pavlis (1991) The Ohio State 1991 Geopotential and Sea Surface Topography Harmonic Coefficient Models, Report No. 410, Department of Geodetic Science and Surveying, The Ohio State University, 45p.
Sandwell, D. T. (1990) Geophysical applications of satellite altimetry, National Report to IUGG 1987-1990, Script Institution of Oceanography, La Jolla, CA.
Sandwell, D. T. (1992) Antarctica marine gravity field from high-density satellite altimetry, Geophys. J. Int., vol. 109, p. 437-448.
Skilbrei, J. (1993) Svalbard Free-air and Bouguer Anomalies, Geological Survey of Norway, 1:1,000,000.
Sobczak, L. W. and D. B. Hearty (1987) Gravity of the Arctic, The Geological Society of America Inc., 1:6,000,000.
von Frese, R. R. B., M. B. Jones, J. W. Kim, and J.-H. Kim (1997) Analysis of Anomaly Correlations, Geophysics, vol.62, No.1, p.342-351.